Run-13 $\psi(2s) \rightarrow \mu^+\mu^-$ with the FVTX

Matt Durham, Melynda Brooks, Hubert van Hecke, Aaron Key,
Ming Liu, Pat McGaughey, Cesar da Silva, Haiwang Yu

May 3, 2014

1 Introduction

The introduction of the Forward Silicon Vertex Tracker (FVTX) in front of the PHENIX muons arms has enhanced the mass resolution of the muon tracking systems to the extent that the excited charmonium state $\psi(2s)$ ($m_{\psi(2s)} \sim$ 3.7 GeV) can now be separated from the larger J/ψ peak ($m_{\psi(1s)} \sim$ 3.1 GeV) in the dimuon mass spectrum, by measuring the dimuon pair opening angle before any multiple scattering occurs in the absorber. This Note describes a measurement of the ratio of $\psi(2s)/\psi(1s)$ mesons at forward rapidity, through their decays to dimuons, from the Run-13 $p + p$ data.

The analysis proceeds as follows: First, the dimuon invariant mass spectrum is found using the momentum measured by the muon tracker, corrected for energy loss in the absorber, and the opening angle found from tracks matched in the FVTX. ROOT's likelihood fitter is used to fit the invariant mass spectrum with a sum of combinatorial background, correlated background, and two peaks which represent the $\psi(1s)$ and $\psi(2s)$ peaks. The integrals of these peak shapes are then corrected for acceptance and trigger efficiency, and the ratio $\psi(2s)/\psi(1s)$ is determined, where many systematic uncertainties cancel. The remaining systematic uncertainties are determined by varying the peak shapes, background shapes, and models used to determine the acceptance correction.

2 Run Selection

To ensure stable performance of the detector that is modeled in simulation, runs which display unusual characteristics are not considered in this analysis. To examine the detector performance, the number of dimuons per event is shown for each run for the North and South arms in Figs. 1 and 2, respectively. Events are from the ((MUIDLL1_N2D||S2D)||(N1D&S1D))&BBCLL1(noVtx) triggered data set, and dimuons are required to satisfy nominal selection criteria (such last lastgap>=3, etc).

A gaussian is fit to the distribution is shown for each arm, and only runs which fall within 3σ are considered in this analysis.

Dimuon Mass Spectra

3 Dimuon Mass Spectra

The mass of each dimuon pair is calculated using the momentum as determined by the muon trackers, with a pair opening angle determined by the FVTX. Since the FVTX is located in front of the hadron absorber, the FVTX measures the muon pair opening angle before any multiple scattering in the absorber

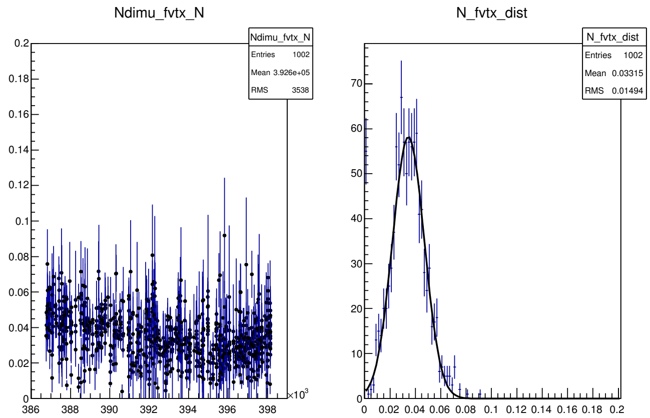

Figure 1: The number of dimuons per event in the North arm as a function of run number (left), and the fitted distribution (right).

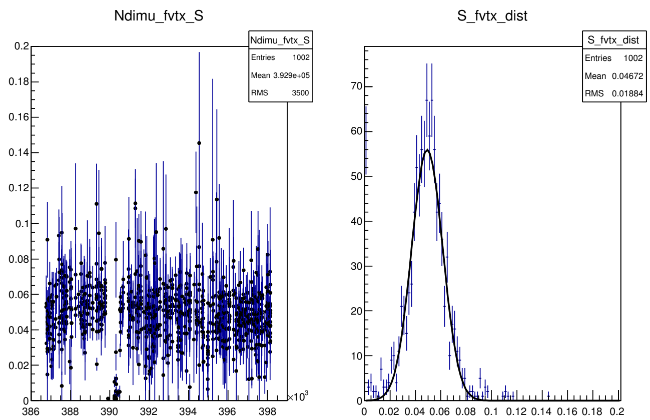

Figure 2: The number of dimuons per event in the South arm as a function of run number (left), and the fitted distribution (right).

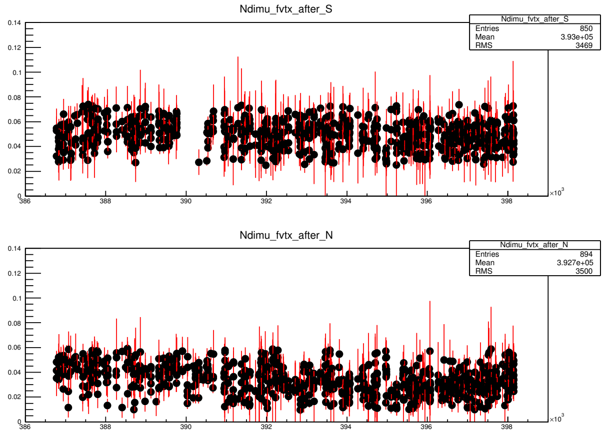

Figure 3: The number of dimuons per event as a function of run number in the South (top) and North (bottom) muons arms, for runs which pass the 3σ good run selection criteria.

material takes place. This location, combined with the small strip size in the FVTX, gives a far superior measurement of pair opening angle (and therefore mass) than is possible with the muon tracking chambers alone.

Muon track candidates are identified using standard muon arm cuts, given in Tab. 1. To be considered in this analysis, tracks must reach at least the third gap in the MuID, have a good match with a MuID road, and have a reasonable chi2 value in the muon arm. Additionally, tracks that form a pair are required to pass through different octants, and at least one track from the pair must have more than 14 hits in the MuTr.

Additional requirements from the FVTX further constrain the tracks and reject background. Track matching between the FVTX and MuTr is considered in the three polar coordinates r, θ, and ϕ. As the deflection due to multiple scattering in the absorber is highly dependent on muon momentum, these cuts are sigmalized in p, and we require matching within 2σ. Identical cuts are used in all simulations shown in this note, unless explicitly stated otherwise.

Variable	Accepted Value
lastgap	$>=3$
DG0	< 10
DDG0	< 9
trchi2	< 10
octant cut	applied
ntrhits	> 14 for at least one track
p_z	> 2 GeV

Table 1: Muon arm cuts (not including the FVTX).

4 Acceptance $\times$ Efficiency Corrections

The dimuon acceptance and detection efficiency is a strong function of the pair's mass and momentum. Previous studies of the dimuon continuum for PPG154 have shown that the acceptance $\times$ efficiency of

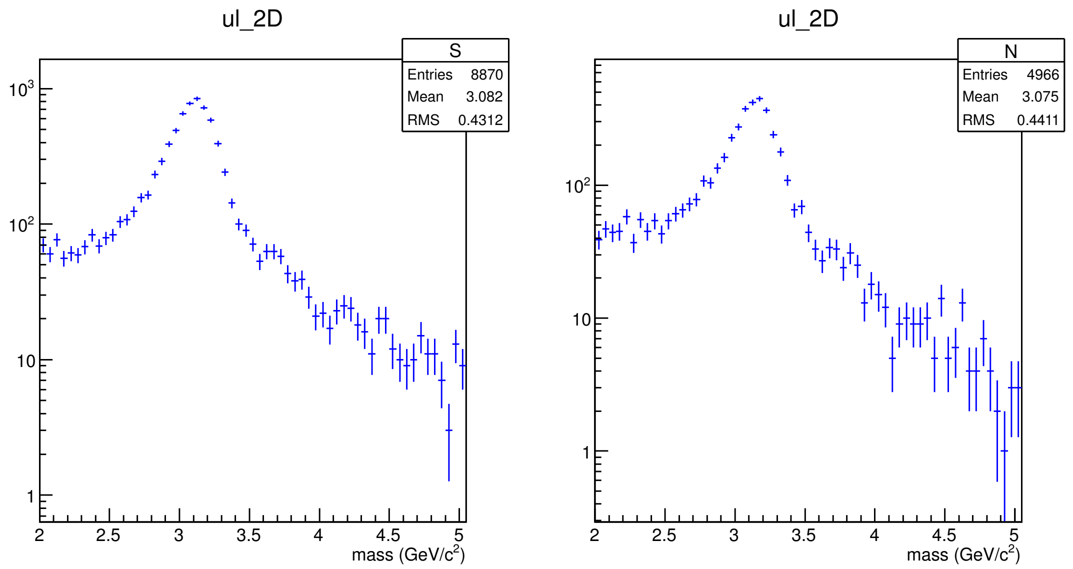

Figure 4: The unlike-sign dimuon mass spectra for the South arm (left) and North arm (right) prepared using the cuts described.

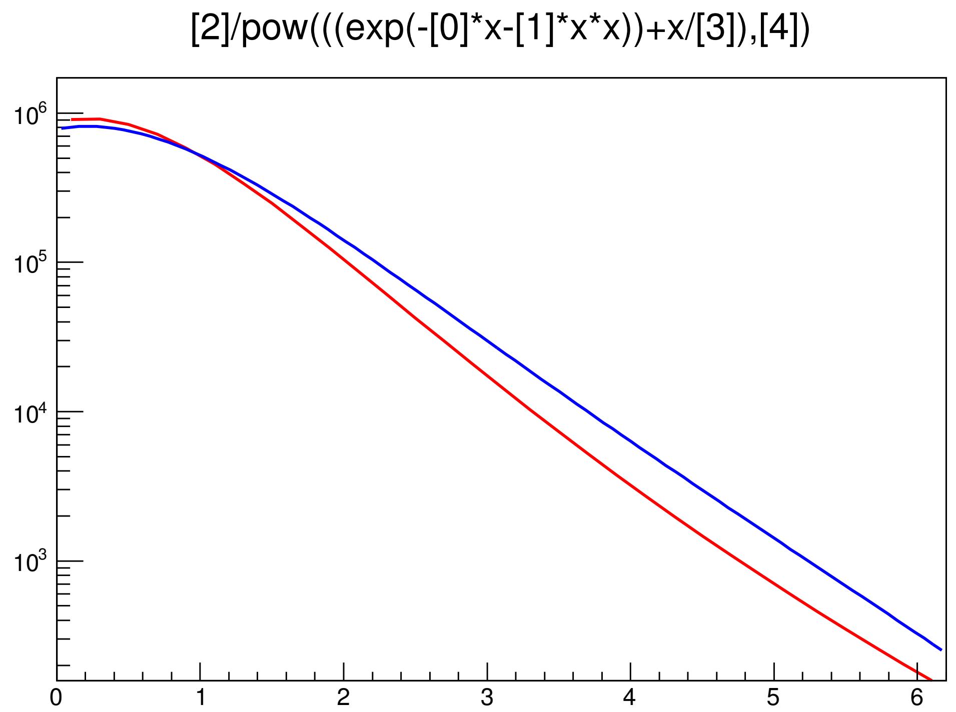

Figure 5: The weighting function for the p_T distribution of generated dimuon pairs, taken from a PYTHIA simulation of $\psi(1s)$ (red) or $\psi(2s)$ (blue) production in $p + p$ collisions at 510 GeV.

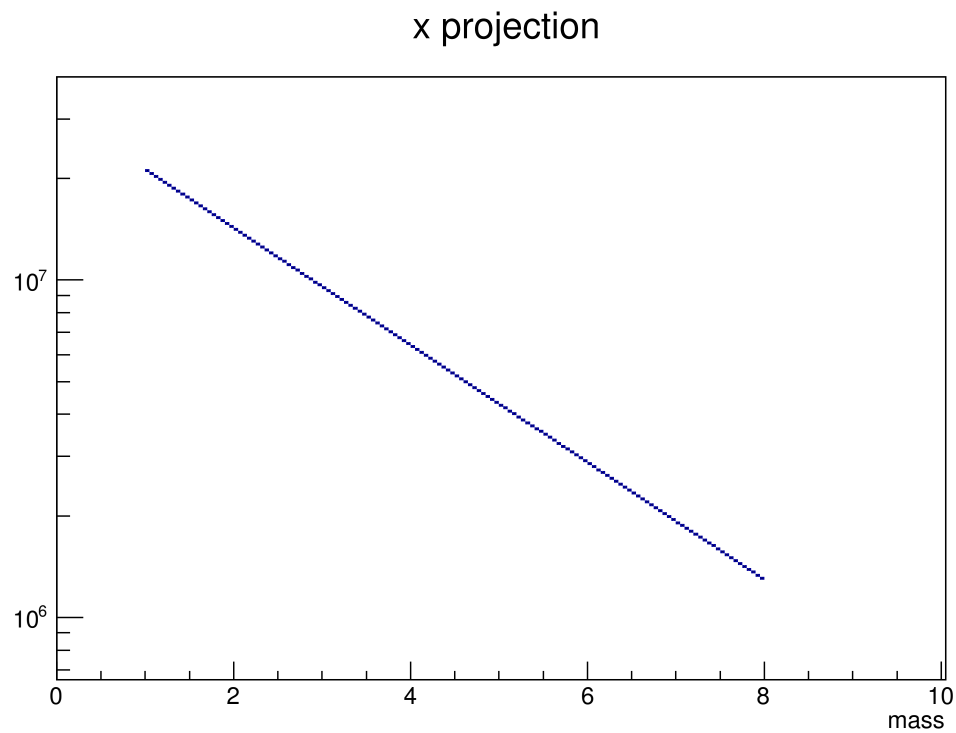

Figure 6: The mass distribution of generated dimuon pairs, taken from the fit to the measured dimuon spectrum in PPG154.

Variable	Accepted Value
dphi_fvtx	$< 2\sigma$
dr_fvtx	$< 2\sigma$
dtheta_fvtx	$< 2\sigma$
chi2_fvtx	< 10
chi2_fvtxmutr	< 10

Table 2: FVTX cuts.

the PHENIX muon arms as a function of mass rises between 2 and 4 GeV/c^2, which indicates that this correction does NOT completely cancel out when making the $\psi(2s)/\psi(1s)$ ratio. Therefore the measured ratio must be corrected by the ratio of the acc$\times$eff value evaluated at the masses of the two particles.

The magnitude of the acc$\times$eff of the muon arms + FVTX is determined with PISA. A realistic distribution of $\mu^+\mu^-$ pairs is used as input to the simulation. The pairs are generated with a p_T range of 0-20, with a weight determined from a fit to the $\psi(1s)$ or $\psi(2s)$ p_T spectrum generated by PYTHIA for $p+p$ collisions at 510 GeV (Fig. 5). The mass distribution of the pairs is taken directly from the measured fully-corrected dimuon pair spectrum from $p+p$ collisions at 500 GeV reported in PPG154 (Fig. 6). The rapidity distribution of the pairs comes from a PYTHIA simulation of pairs which enter the muon arm solid angle, and the z-vertex distribution is a Gaussian with a width determined by a fit to the data (see Fig.7 for the generated distribution and Fig. 8 for the fit to the data). Note that the generated distributions are all wider than the actual distributions in data considered in this analysis, to account for any potential edge-type effects.

After generation, the pairs are put through the standard pisa and pisaToDST reconstruction chain to produce dimuon pDSTs. These simulated data files are then put through the same analysis programs as the real data, where all the same cuts are applied. The ratio of the output to the generated input spectra therefore represents the fraction of dimuon pairs that are accepted in the FVTX+muon arms and survive all analysis cuts.

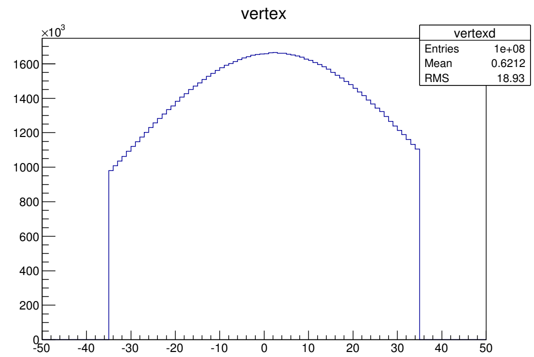

Figure 7: The z vertex distribution of generated dimuon pairs.

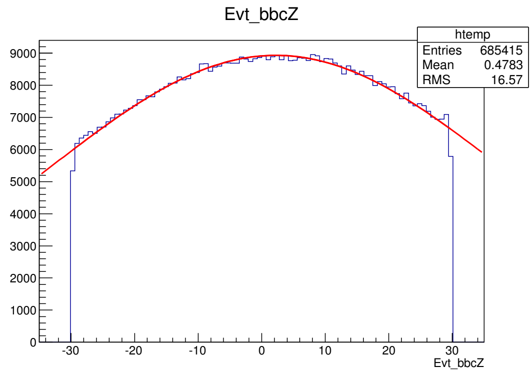

Figure 8: The fitted z vertex distribution of dimuon pairs from the 2D triggered data set.

The mass-dependent acceptance $\times$ efficiency correction for the South and North muon arms are shown in Fig. 9. For the $\psi(2s)/\psi(1s)$ ratios that are the focus of this analysis, the correction is the ratio of the values of the fits at the $\psi(1s)$ and $\psi(2s)$ masses. The value of this correction is 0.69 in the South arm and 0.77 in the North arm. To determine a systematic uncertainty, the simulation is re-run with the p_T and rapidity weighting from the PHPYTHIA simulation of $\psi(2s)/$ mesons. In this case the relative correction factors are found to be 0.693 and 0.768, very close to what was measured with the $\psi(1s)$ parameterizations. The difference is rounded up to 1% and taken as the systematic uncertainty on the relative acceptance correction.

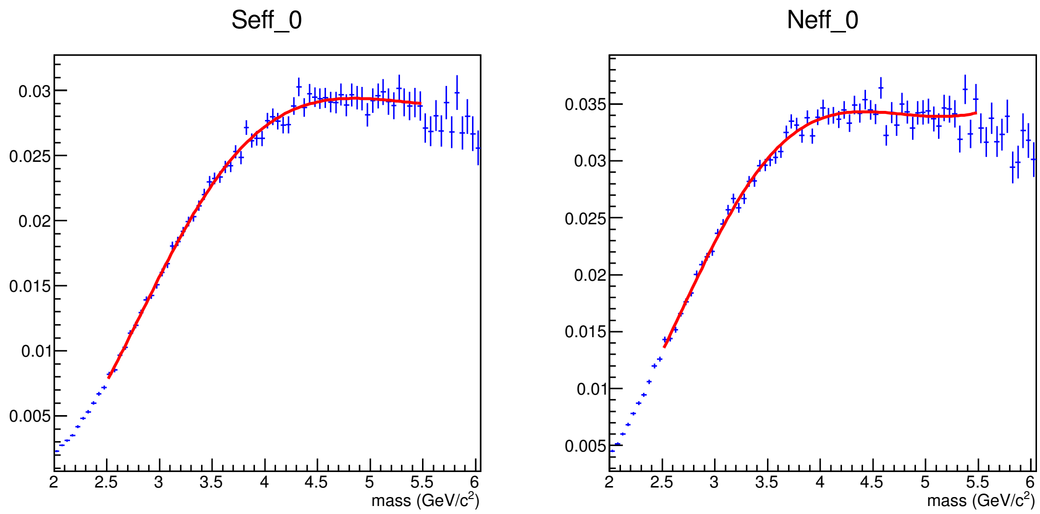

Figure 9: The mass-dependent acceptance $\times$ efficiency correction for the South (left) and North muon arms, from dimuon pairs generated from parameterizations of $\psi(1s)$ spectra.

Additional mass-dependent efficiencies are introduced by the 2D dimuon trigger that is used in this analysis (which requires two tracks the penetrate to at least the third MuID gap). To examine these effects, the dimuon mass spectrum is prepared for events which satisfy Minimum Bias trigger data, and the subset of the those events in the MB triggered dataset which also satisfied the 2D trigger. These mass distributions are shown in Fig10. The ratio of these two mass spectra is the 2D trigger efficiency, shown in Fig 11.

The fit shown in Fig. 11 is used to determine the magnitude of the correction. Again, for the purposes here, only the relative correction at the $\psi(2s)$ and $\psi(1s)$ masses is important. For the North arm, the correction is 0927 (i.e. a 7.3% change), and for the South arm it is 0.951(a change of 4.9%). A conservative systematic uncertainty of 50% is assigned to the small change this correction causes in the $\psi(2s)/\psi(1s)$ ratio.

4.1 PHPYTHIA .cfg files

The configuration file used to generate $\psi(1s)$ mesons:

```
roots   510
proj    p
targ    p
frame   cms
msel    0       // turn on all production mechanisms manually

msub 86 1 // g+g->j/psi
msub 106 1 // g+g->j/psi+gamma
```

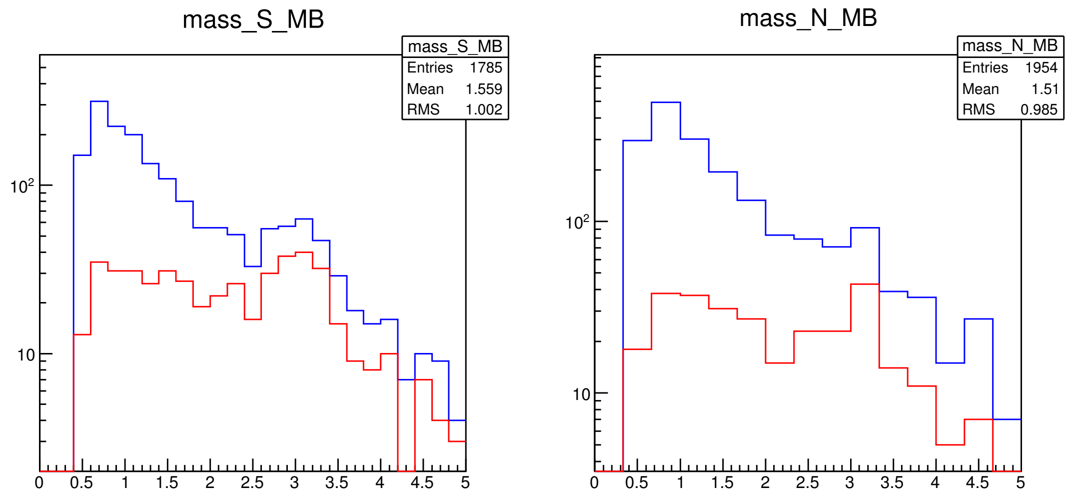

Figure 10: Dimuon mass spectra from the Min Bias triggered data set (blue), for the South (left) and North (right) muon arms. The mass spectra from the subset of these events which also fire the 2D dimuon trigger is shown in red.

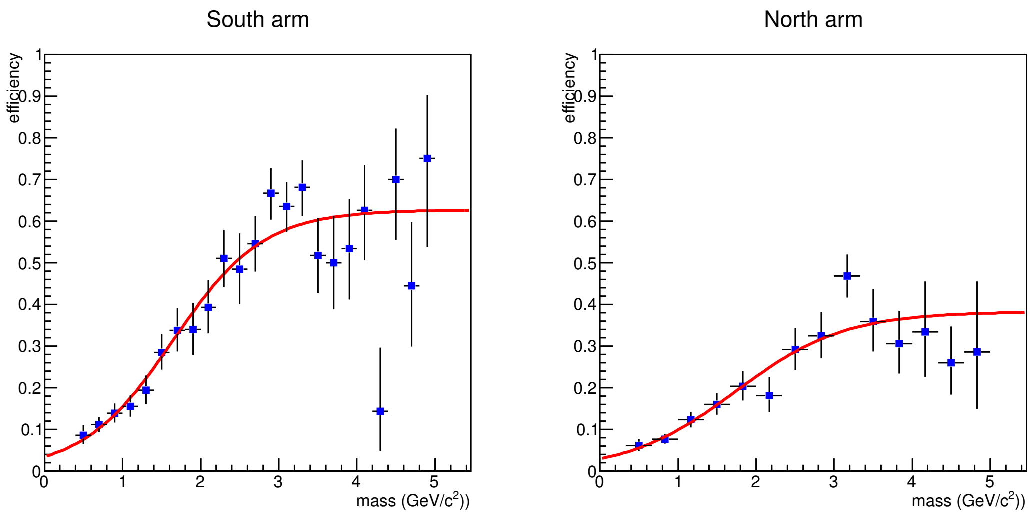

Figure 11: Ratio of the two mass spectra shown in Fig. 10, which represents the 2D trigger efficiency.

```
msub 107 1 // g+gamma->j/psi+g
msub 108 1 // gamma+gamma->j/psi+gamma

mdme 858 1 0 // J/Psi -> ee turned OFF
mdme 859 1 1 // J/Psi -> mumu turned ON
mdme 860 1 0 // J/JPsi -> random turned OFF

//mstp 51 7 // structure function for CTEQ5L

//the following lines to use CTEQ6 from cesar
mstp    52 2  // usa LHAPDF
mstp    54 2
mstp    56 2
mstp    51 10041 // CTEQ6LL
```

The configuration file used to generate $\psi(2s)$ mesons:

```
roots   510
 proj    p
 targ    p
 frame   cms

 msel    0     // turn on all prod. mechanisms manually

 msub    86 1  // g+g->j/psi
 msub    106 1   // g+g -> J/psi+gamma turned ON
 msub    107 1   // g+gamma -> J/psi+g turned ON
 msub    108 1   // gamma+gamma->J/psi+gamma turned ON

 kfpr    86  1 100443 // request PsiPrime (2s) instead of psi for process 86
 kfpr    106 1 100443 // request PsiPrime (2s) instead of psi for process 106
 kfpr    107 1 100443 // request PsiPrime (2s) instead of psi for process 107
 kfpr    108 1 100443 // request PsiPrime (2s) instead of psi for process 108

 mdme   1567 1 0   // psi' -> ee turned OFF
 mdme   1568 1 1   // psi' -> mumu turned ON
 mdme   1569 1 0   // psi' -> random turned OFF

 // you have to use the library /direct/phenix+u/workarea/slash/pythia/libPythia6PDF.
 mstp    52 2   // use LHAPDF
 mstp    54 2
 mstp    56 2
 mstp    51 10041 // structure function for CTEQ6LL
```

5 Combinatorial Backgrounds

Two standard methods were investigated to determine the magnitude of the uncorrelated backgrounds under the ψ and ψ' peaks in the dimuon invariant mass spectrum: the like-sign method, which uses pairs of muons with the same charge produced in an event, and the mixed event method, which constructs pairs from muons produced in different events that have similar characteristics.

5.1 Like-sign Background

Using events which satisfied the same cuts used to find the unlike-sign dimuon invariant mass spectrum, the like-sign invariant mass spectrum was found for $\mu^+\mu^+$ and $\mu^-\mu^-$ pairs. The like-sign mass spectrum is normalized following the standard PHENIX methods:

$$Normalization_{ls} = \frac{2\sqrt{N_{++}N_{--}}}{N_{++}+N_{--}} \tag{1}$$

5.2 Mixed Event Backgrounds

To overcome the statistical limitations of the like-sign background subtraction methods, we use event mixing to construct a mass spectrum of muon pairs using muons produced in different events. The contributions to the spectrum are purely combinatorial, and can have no contributions from correlated dimuon emission. Following the methods used in PPG142/AN890 (where they had a similar problem with a low statistics like-sign background), the mixed events are normalized to the like-sign by the factor:

$$Normalization_{mixed} = \frac{2\sqrt{N_{++}N_{--}}}{N_{+-}^{mix}} \tag{2}$$

where N_{+-}^{mix} is the number of unlike-sign pairs from the mixed events. A systematic uncertainty from this normalization factor is determined by varying the mass range over which the factor is calculated, see Tab. 5 and the related discussion for details.

6 Peak Extraction

After the dimuon mass spectrum is prepared with the cuts described previously, a fit to the raw unlike-sign counts is used to extract the peaks corresponding to the $\psi(1s)$ and $\psi(2s)$ states. The total fit function includes the properly normalized mixed event combinatorial background, an exponential function to represent the correlated background dimuons, and peaks to represent the resonances. Each of the signal peaks is represented by the sum of a Gaussian and a Crystal Ball function (which itself is a Gaussian core with a power law tail to the low side that accounts for muon pairs that are reconstructed with an erroneously low mass due to range straggling in the absorber).

The Crystal Ball function is explained pretty well here:
$https://www.jlab.org/primex/weekly\_meetings/slides\_2009\_07\_17/dmitry/crystalball.html$
The fit parameters are defined as follows:

p0 - Crystal Ball parameter α,

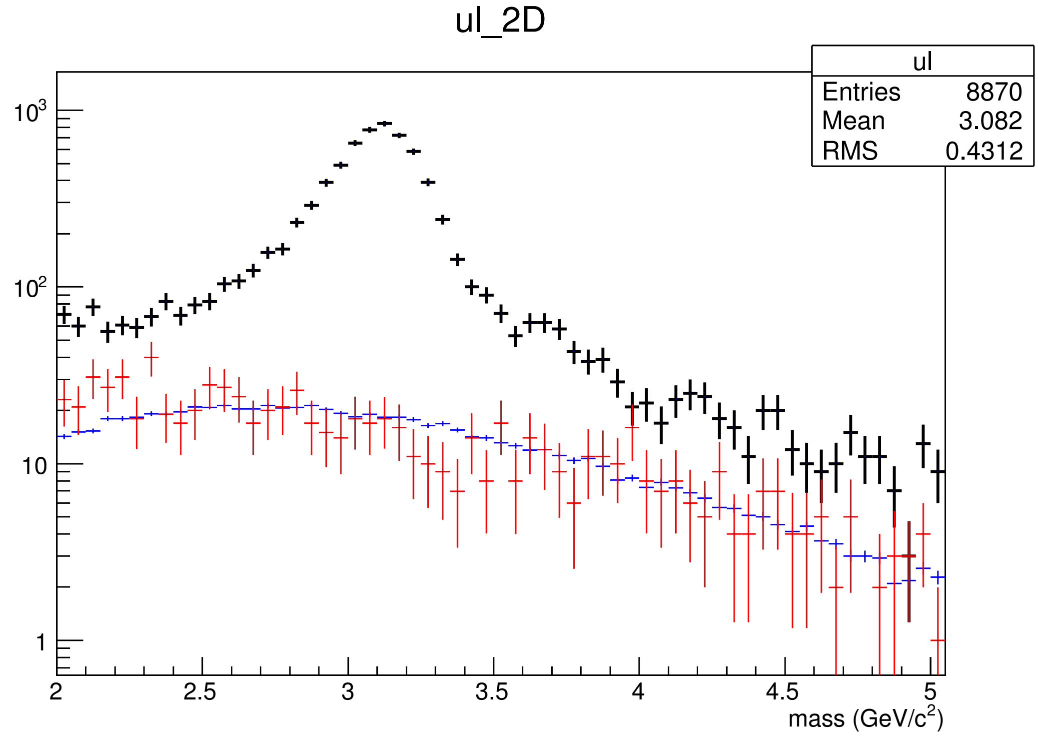

Figure 12: The unlike-sign dimuon mass spectra for the south arm (black), with two estimations of the combinatorial background, from like-sign events in red and mixed events in blue.

p1 - Crystal Ball parameter n,
p2 - $\psi(1s)$ Crystal Ball parameter μ,
p3 - $\psi(1s)$ Crystal Ball parameter σ,
p4 - $\psi(1s)$ Crystal Ball parameter N,
p5 - Gaussian parameter N,
p6 - $\psi(2s)$ Crystal Ball parameter N,
p7 - Exponential background normalization,
p8 - Exponential background slope

There are several constraints on the fit function. Since both resonance peaks are expected to display similar effects from straggling in the absorber, the Crystal Ball parameters α and n which define the low mass tail are set to be the same. The width of the $\psi(2s)$ peak is expected to be wider than the $\psi(1s)$ peak, due to the fact that the higher mass and harder p_T spectrum of the 2s state will produce higher momentum decay muons, which have a larger uncertainty in reconstructed momentum in the spectrometer. The ratio of widths of the $\psi(2s)$ to $\psi(1s)$ is set to be 1.15, in accordance with simulation, and varied to determine a systematic uncertainty (see Tab3 and related discussion). The difference between the centroids of the $\psi(2s)$ and $\psi(1s)$ peaks is set to the PDG value of 589 MeV/c^2.

The second gaussian under each peak is set to be centered at the same mass as the Crystal Ball function. The relative normalization of the second gaussian to the Crystal Ball function is set to be the same for both resonances, since they should have the same line shape. The width of the second gaussian is set to 200 MeV in the nominal fit case, and varied to determine a systematic uncertainty (see Tab4 and related discussion).

Fig. 13 shows the fit to the unlike sign sign dimuon mass spectrum. The mixed event background is shown by the blue points, and the total background (consisting of the mixed events histogram plus an exponential) is shown in red. The ratio of the data to the fit is given in Fig. 13. Similar plots are shown for the South arm in Figs. 15 and 16. The North arm data is insufficiently precise to constrain the Crystal Ball fit parameters α and n, so they are set to the parameters determined by the fit to the South arm data. Since these parameters describe the low mass tail of the resonances due to range straggling, and the absorber in both the North and South arms is nearly identical, this is a well-motivated constraint.

After fitting, the integral of the CB+Gaussian peak function for each resonance is calculated, then corrected for the acceptance and trigger efficiency. The values obtained for the South and North arms are $\psi(2s)/\psi(1s)$ = 2.59±0.41$\%$ and 3.45±0.67$\%$, respectively. A comparison to world data is given in Fig. 17.

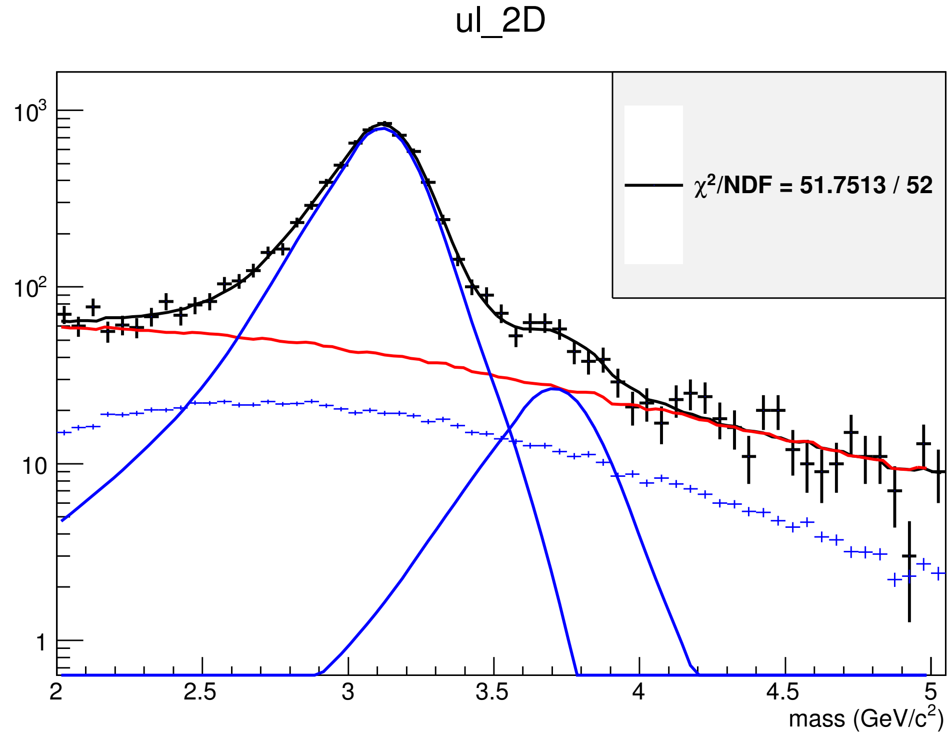

Figure 13: The unlike-sign dimuon mass spectrum for the South arm (black), with fit (see text for details). The blue points are the mixed event combinatorial background.

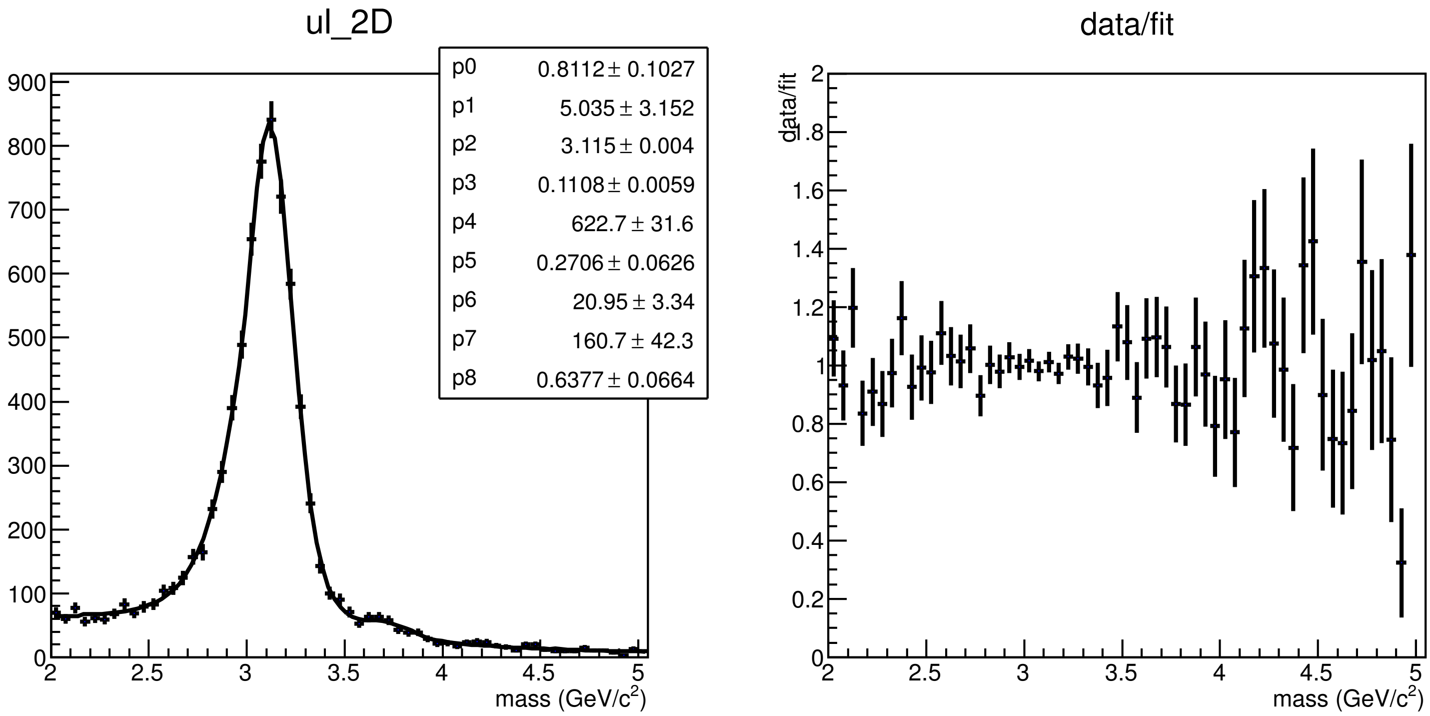

Figure 14: Ratio of data point to total fit function value for the South arm.

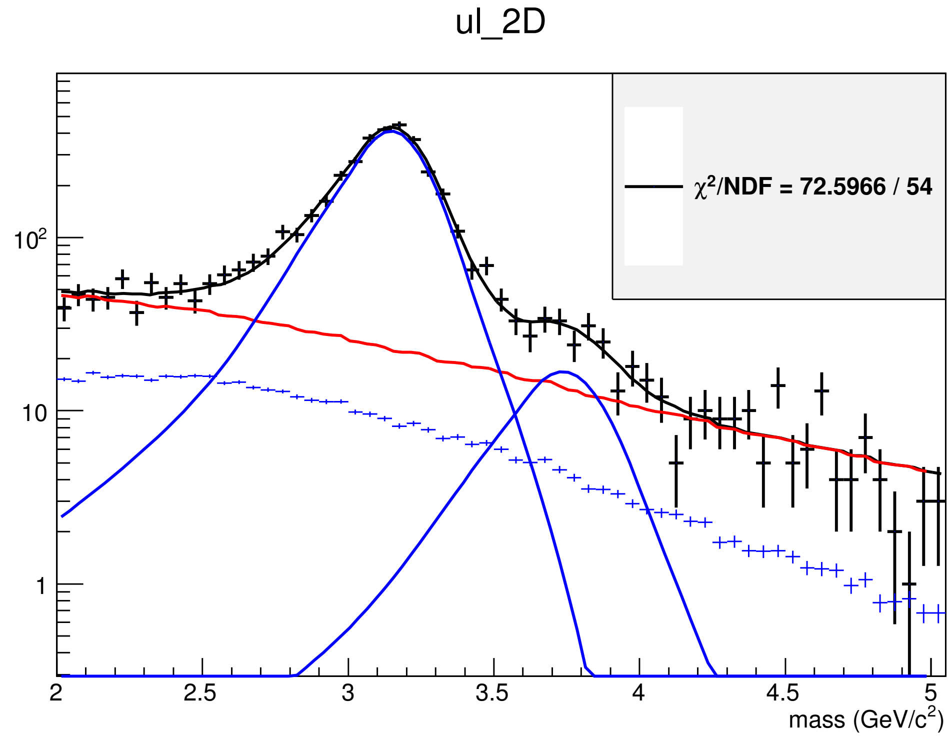

Figure 15: The unlike-sign dimuon mass spectrum for the North arm (black), with fit (see text for details).

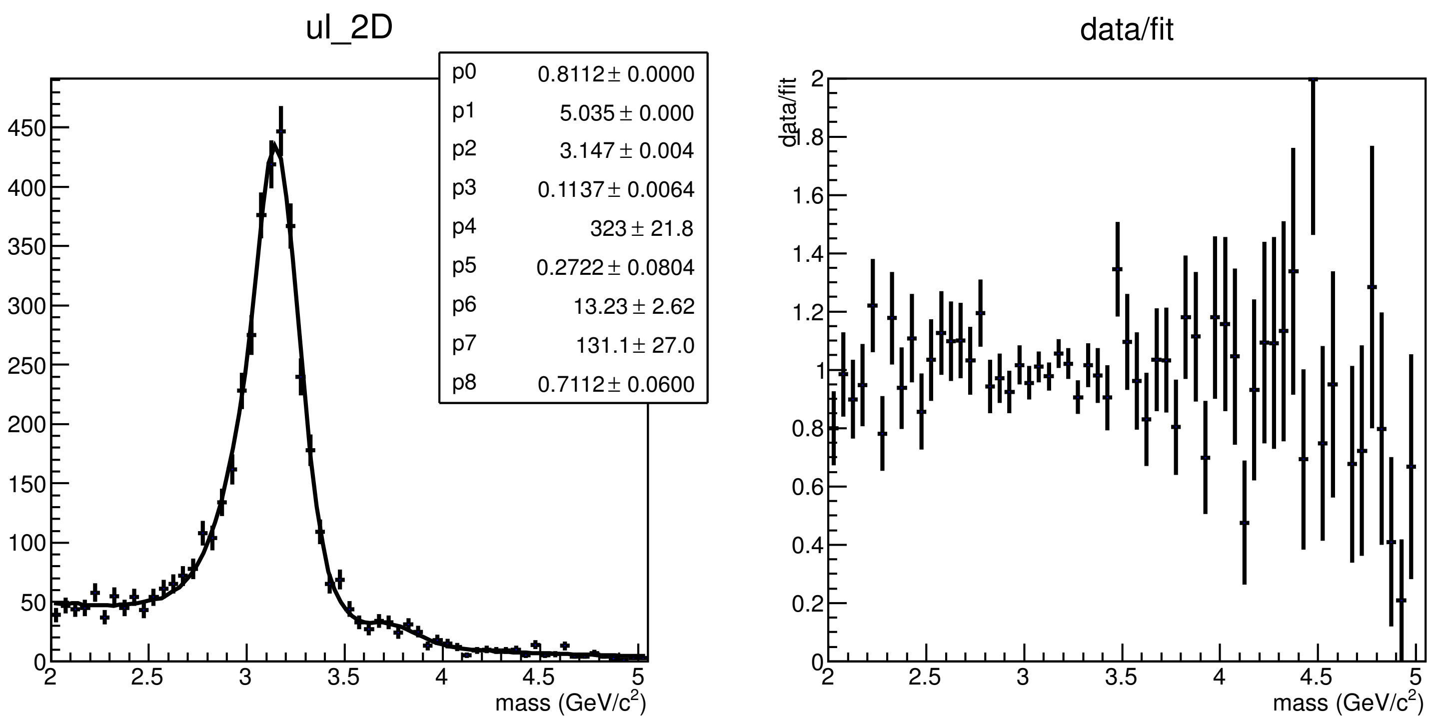

Figure 16: Ratio of data point to total fit function value for the North arm.

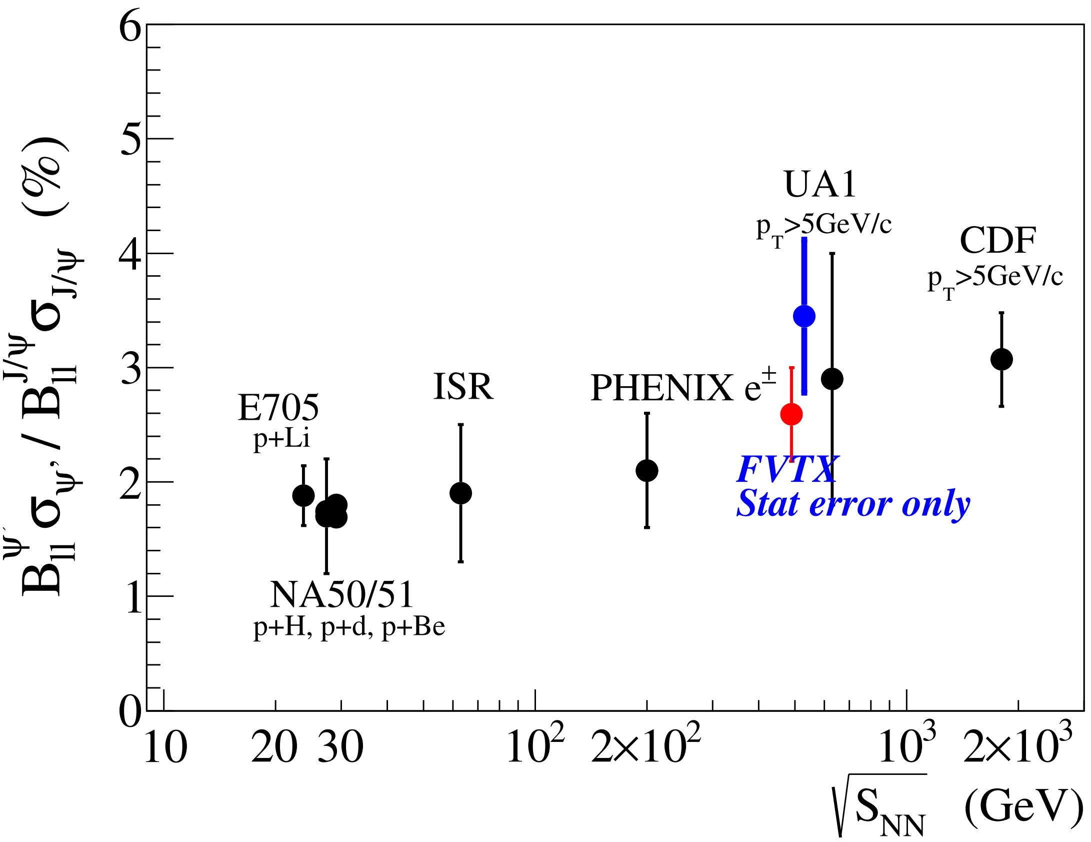

Figure 17: The p_T-integrated $\psi(2s)/\psi(1s)$ ratio for the North arm (blue) and the South arm (red) compared to world data. The data points are slightly displaced from 510 GeV for clarity.

The fit function has several constraints which are adjusted to determine systematic uncertainties. The width of the $\psi(2s)$ peak is nominally set to be $1.15\times$ the width of the $\psi(1s)$ peak, following results from simulation. From calculations in the PHENIX NIM paper, the ratio of the widths should be 1.1, which is taken as a lower bound. The upper bound is set the same distance from the midpoint as the lower bound, at 1.20. The constraint is adjusted and the spectra are re-fit. The result fits and χ^2 values are shown in Figs. 18 through 21. The fully corrected $\psi(2s)/\psi(1s)$ ratio for each case is collected in Tab. 3, along with the statistical uncertainty on the ratio. We note here that the statistical uncertainties for each case are highly correlated, since the same data is being fit. The uncertainties are given for completeness.

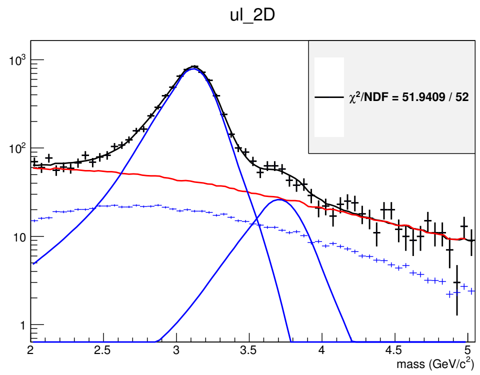

Figure 18: Fit to the South arm dimuon mass spectrum, with the constraint on the ratio of the $\psi(2s)$ to $\psi(1s)$ peak widths set to 1.20.

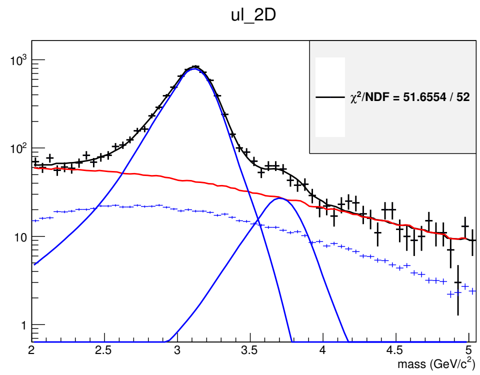

Figure 19: Fit to the South arm dimuon mass spectrum, with the constraint on the ratio of the $\psi(2s)$ to $\psi(1s)$ peak widths set to 1.10.

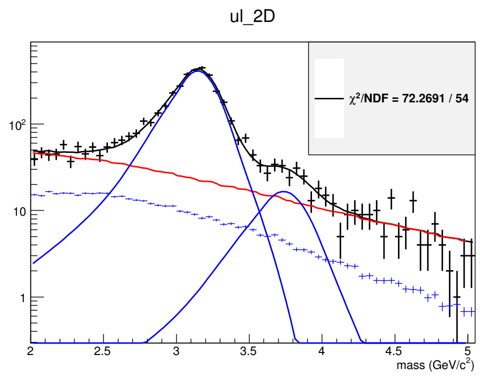

Figure 20: Fit to the North arm dimuon mass spectrum, with the constraint on the ratio of the $\psi(2s)$ to $\psi(1s)$ peak widths set to 1.20.

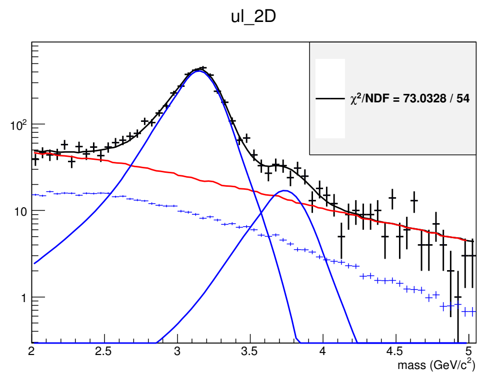

Figure 21: Fit to the North arm dimuon mass spectrum, with the constraint on the ratio of the $\psi(2s)$ to $\psi(1s)$ peak widths set to 1.10.

In the South arm, varying the ratio of the peak widths down to 1.1 and up to 1.2 changes the fully corrected $\psi(2s)/\psi(1s)$ ratio by -2.7% and +2.3%, respectively. In the North arm, adjustments of the fit constraint change the value by $\pm 2.9\%$. The average of the variance due to this change is taken as the systematic uncertainty due to this constraint on the fit function, as 2.5% for the South arm and 3% for the North arm.

$\sigma(2s)/\sigma(1s)$	South Arm $\psi(2s)/\psi(1s)$	North Arm $\psi(2s)/\psi(1s)$
1.15	2.59±0.41%	3.45±0.67%
1.10	2.52±0.41%	3.35±0.66%
1.20	2.65±0.41%	3.55±0.69%

Table 3: Variation in ratio due to assumption on the ratio of the peak widths. The first entry in the table is for the nominal fitting case as shown in Figs. 13 and 15.

A similar approach is used to determine the systematic uncertainty on the $\psi(2s)/\psi(1s)$ ratio due to the constraint on the width of the second gaussian under both peaks. If the width is not constrained, the second gaussian blows up to unphysically large values. The effect of varying the width of the second gaussian up to 225 MeV and down to 175 MeV is shown in Figs 22 through 25. The effect on the fully corrected $\psi(2s)/\psi(1s)$ ratio is given in Tab. 4. From the change due varying the constraint on the second gaussian width, a systematic uncertainty of 10% and 12% is set on the $\psi(2s)/\psi(1s)$ ratio in the Sout hand North arms, respectively.

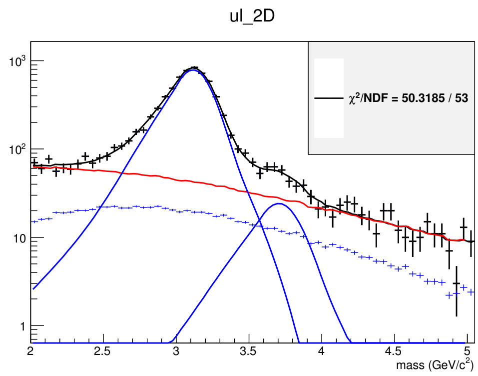

Figure 22: Fit to the South arm dimuon mass spectrum, with the second gaussian peak width set to 225 MeV.

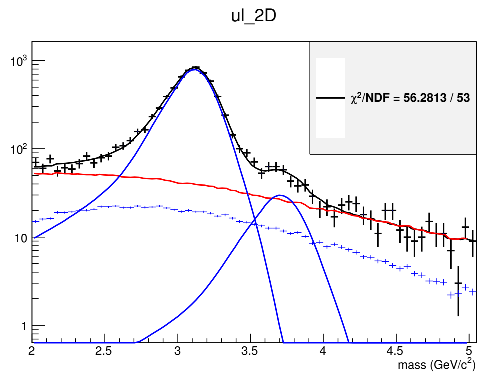

Figure 23: Fit to the South arm dimuon mass spectrum, with the second gaussian peak width set to 175 MeV.

Second Gaussian Width	South Arm $\psi(2s)/\psi(1s)$	North Arm $\psi(2s)/\psi(1s)$
200 MeV	2.59±0.41%	3.45±0.67%
225 MeV	2.36±0.38%	3.11±0.64%
175 MeV	2.89±0.44%	3.92±0.72%

Table 4: Variation in ratio due to assumption on the width of the second Gaussian. The first entry in the table is for the nominal fitting case as shown in Figs. 13 and 15.

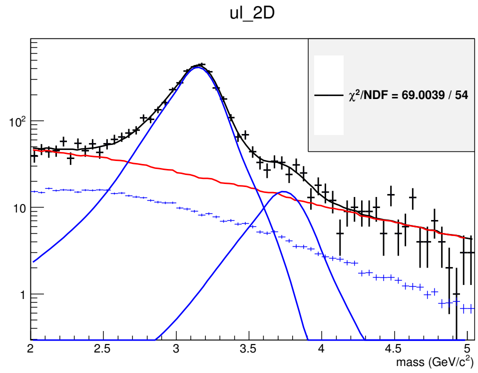

Figure 24: Fit to the North arm dimuon mass spectrum, with the second gaussian peak width set to 225 MeV.

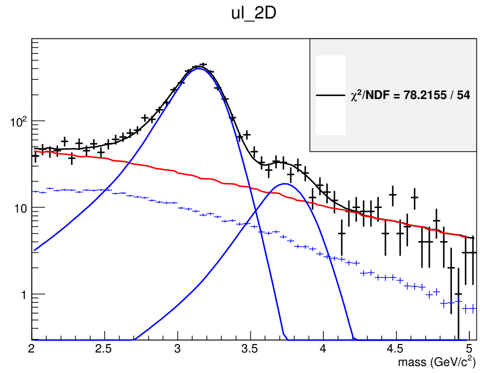

Figure 25: Fit to the North arm dimuon mass spectrum, with the second gaussian peak width set to 175 MeV.

As previously discussed, the normalization for the mixed event background is found by a comparison to the like-sign counts in a set mass range. Here, that mass range is varied to determine an uncertainty due to that normalization factor. The relevant fits are shown in Figs 26 through 29, and the results on the fully corrected $\psi(2s)/\psi(1s)$ ratio are given in Tab. 5. Systematic uncertainties of 3% are assigned to both the South and North arms.

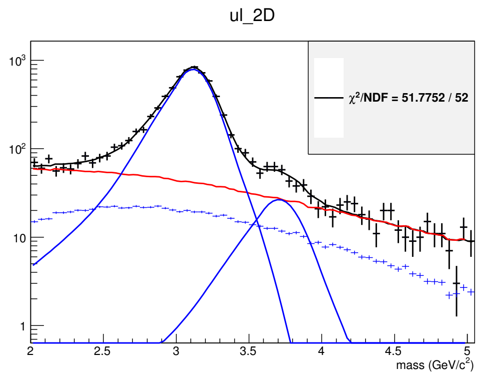

Figure 26: Fit to the South arm dimuon mass spectrum, with mixed events normalized over the mass range 2-5 GeV.

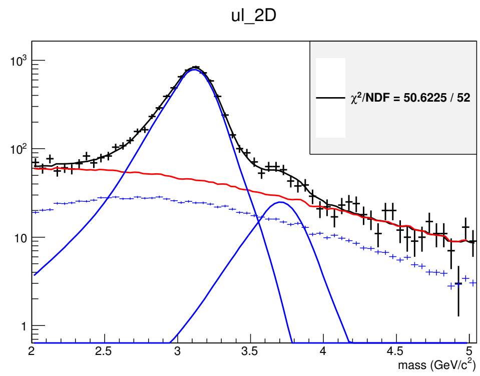

Figure 27: Fit to the South arm dimuon mass spectrum, with mixed events normalized over the mass range 1.5-4 GeV.

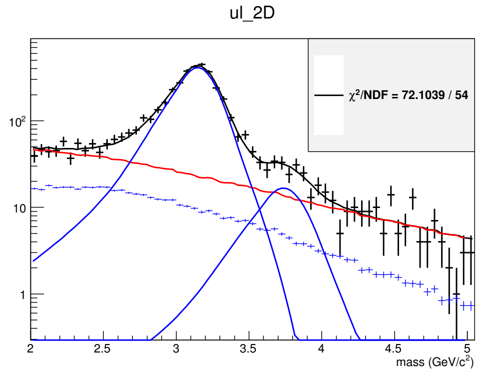

Figure 28: Fit to the North arm dimuon mass spectrum, with mixed events normalized over the mass range 2-5 GeV.

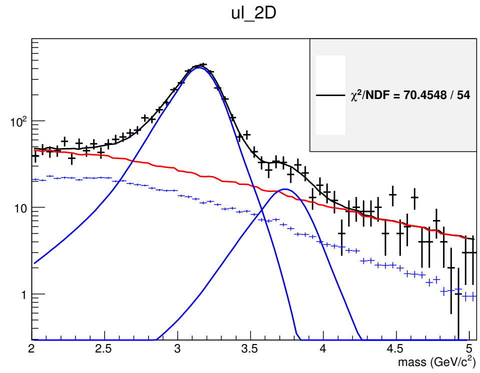

Figure 29: Fit to the North arm dimuon mass spectrum, with mixed events normalized over the mass range 1.5-4 GeV.

Mass Range	South Arm $\psi(2s)/\psi(1s)$	North Arm $\psi(2s)/\psi(1s)$
2-4 GeV	2.59±0.41%	3.45±0.67%
1.5-4 GeV	2.43±0.40%	3.34±0.66%
2-5 GeV	2.59±0.40%	3.43±0.67%

Table 5: Variation in ratio due to mass range used for mixed event combinatorial background normalization. The first entry in the table is for the nominal fitting case as shown in Figs. 13 and 15.

The slope and normalization of the exponential that represents the correlated backgrounds is likely sensitive to the range over which it is fit in mass. The range of the entire fit is therefore varied from the nominal 2-5 GeV to examine this dependency. Relevant fits are shown in Figs. 30 through 33, and the results on the fully corrected $\psi(2s)/\psi(1s)$ ratio are given in Tab. 6. Systematic uncertainties of 7% and 3% are assigned to the South and North arms, respectively.

Mass Range	South Arm $\psi(2s)/\psi(1s)$	North Arm $\psi(2s)/\psi(1s)$
2-5 GeV	2.59±0.41%	3.45±0.67%
1.5-5 GeV	2.86±0.43%	3.63±0.62%
2-6 GeV	2.67±0.40%	3.49±0.66%

Table 6: Variation in ratio due to mass range used for fitting. The first entry in the table is for the nominal fitting case as shown in Figs. 13 and 15.

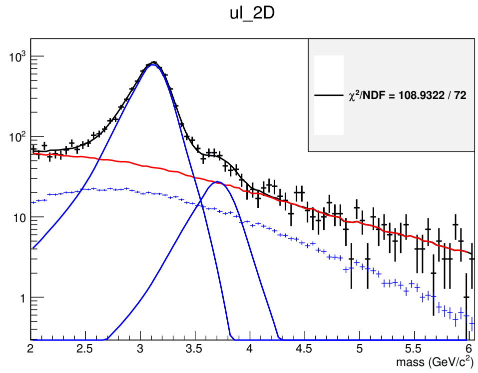

Figure 30: Fit to the South arm dimuon mass spectrum over the mass range 2-6 GeV.

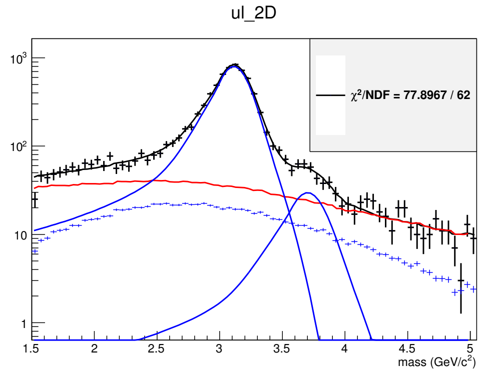

Figure 31: Fit to the South arm dimuon mass spectrum over the mass range 1.5-5 GeV.

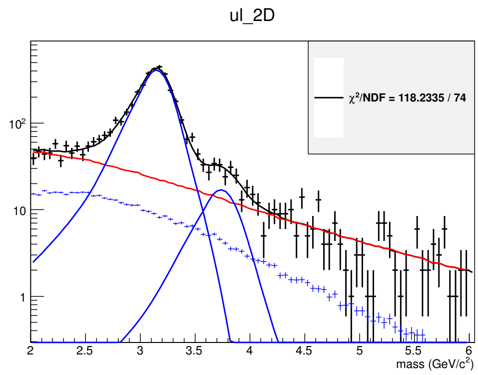

Figure 32: Fit to the North arm dimuon mass spectrum over the mass range 2-6 GeV.

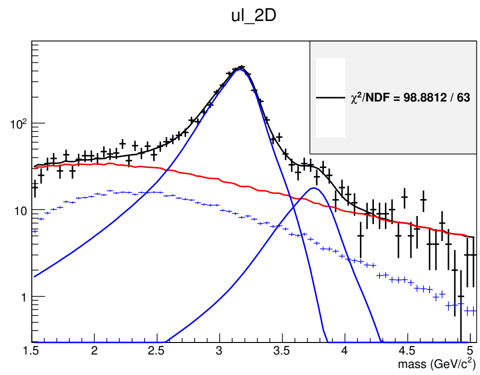

Figure 33: Fit to the North arm dimuon mass spectrum over the mass range 1.5-5 GeV.

A summary of the sources of systematic uncertainties and their values is given in Tab. 7.

7 Results

The p_T integrated ratios of the yields of $\psi(2s)/\psi(1s)$ to dimuons as measured in the North and South arms are R = 2.59±0.41(stat) ±0.34(sys) $\%$ and 3.45±0.67±0.48(sys)$\%$, respectively.

As the North and South arms are treated independently throughout this analysis, the conservative assumption is to treat the uncertainties as completely uncorrelated. The two data points are combined according to the method used by the PDG for combining separate measurements of the same quantity. The final average data point is R = 2.84 $\pm$ 0.45, shown in Fig. **??**.

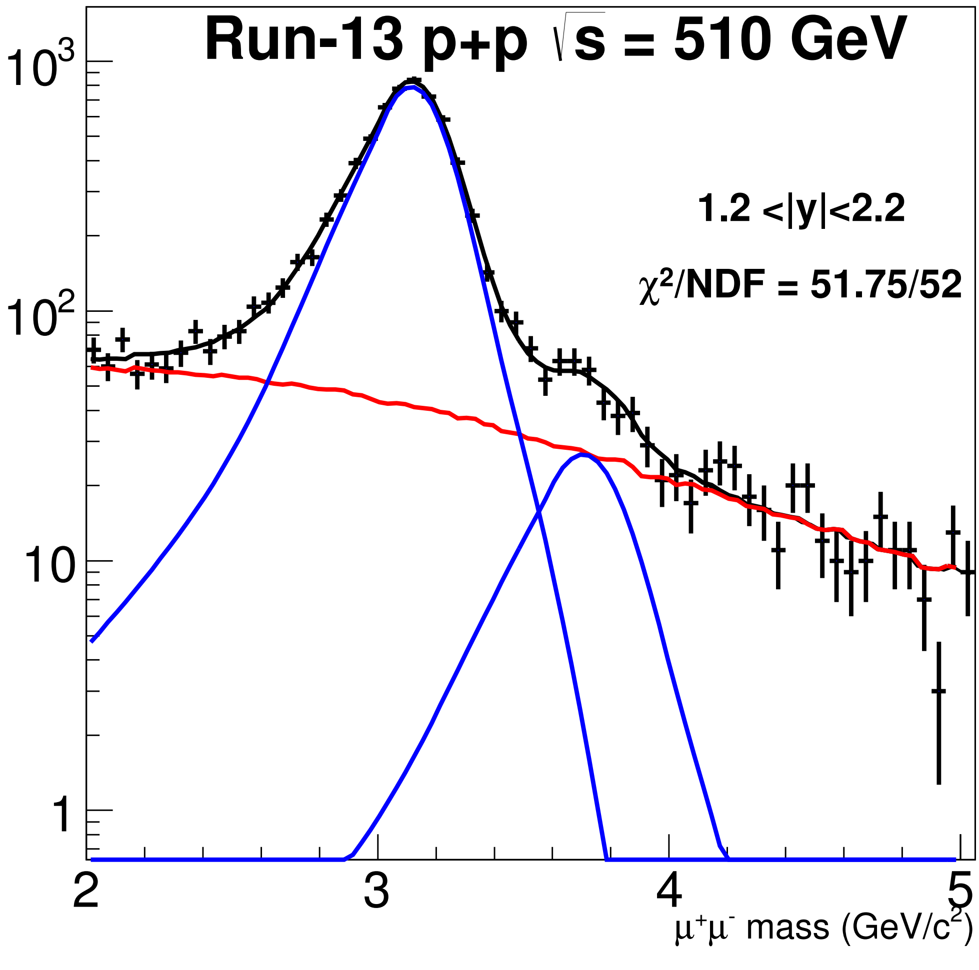

Figure 34: The fit to the South arm dimuon spectrum, preliminary result.

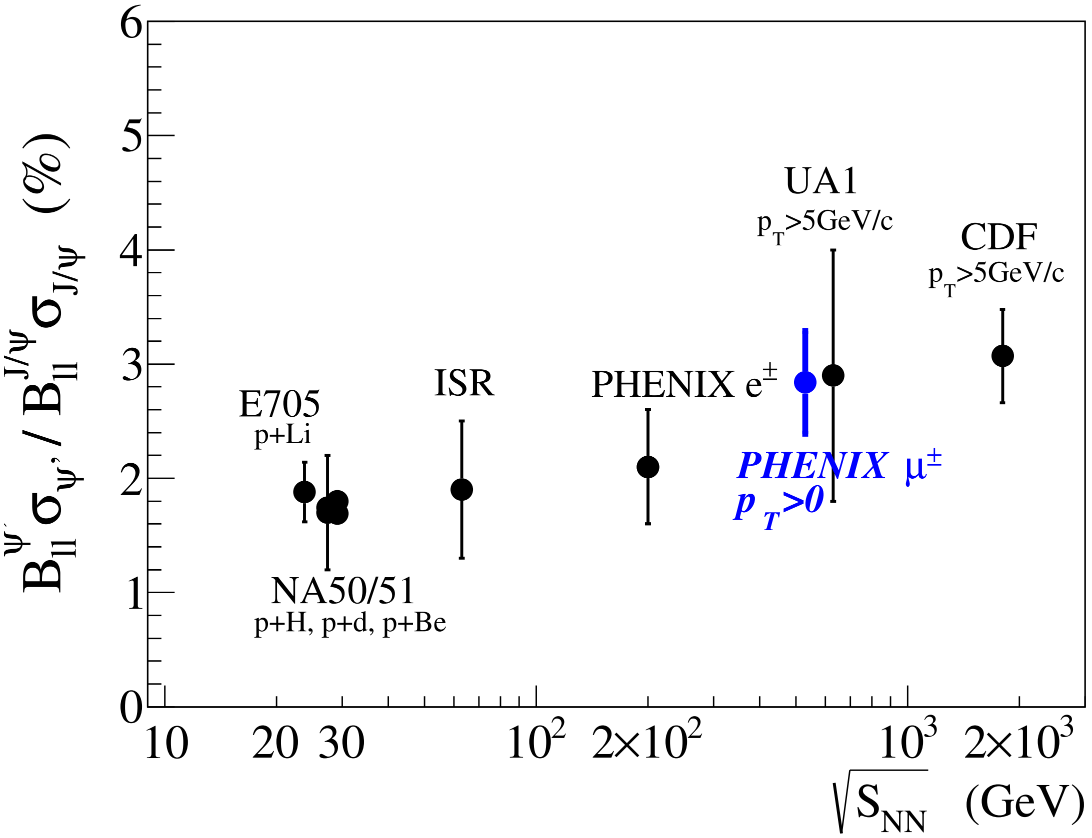

Figure 35: The combined 2s/1s ratio, preliminary result.

Uncertainty	South Arm	North Arm
$\sigma(2s)/\sigma(1s)$ constraint	2.5%	3%
Second Gaussian width constraint	10%	12%
Mixed Event Normalization	3%	3%
Background Fit Mass Range	7%	3%
Trigger Efficiency	2.5%	4%
Acceptance correction	1%	1%
TOTAL	13%	14%

Table 7: Summary of systematic uncertainties.